Proceedings of the 9th International Conference on Information Technology and Applications in Biomedicine, ITAB 2009, Larnaca, Cyprus, 5-7 November 2009

Active Shape Model Aided by Selective Thresholding for Lung Field Segmentation in Chest Radiographs

Dimitris K. Iakovidis, *Member, IEEE* and Michalis Savelonas, *Member, IEEE*

Abstract—**Active shape models (ASMs) are statistical, deformable models, exhibiting a remarkable performance for the segmentation of the lung fields in plain chest radiographs. In this paper we propose a novel approach to improving the robustness of the original ASM against weak lung field boundaries, which can cause leaking of the shape's contour into the lung fields. The ASM is shielded against leaking by the prior application of a grey-level selective thresholding scheme that subtracts irrelevant anatomic structures from the radiograph. The proposed approach copes with affine lung field projections and features resistance to the presence of dense external objects used for patient's monitoring and support. Its advantageous performance is demonstrated on a challenging set of chest radiographs obtained from patients with bacterial pulmonary infections.**

Index Terms— *Active Shape Models, Chest Radiographs, Bacterial Infection*

I. Introduction

Historically, one of the first research challenges taken in the field of medical image processing and analysis is the segmentation of chest radiographs into regions of projected anatomic structures. Since the early sixties [7] a significant effort has been invested to the development of various methodologies tackling with the delineation of complex structures such as the lung fields, the ribs, the clavicles, and the heart [1],[9]. However, there are still many open issues to be resolved, especially when it comes to a real-world application level.

In the case of the lung field segmentation, an issue that has not received much attention is the delineation of the lung fields in the presence of abnormalities affecting the visibility of their boundaries. Such abnormalities may appear as a result of a bacterial pulmonary infection and can make the lung field boundaries hardly visible even by experienced physicians [2],[3]. Methodological approaches that cope with this kind of abnormalities have been based on active shape models (ASMs) [4],[5], on graph cuts [6], and on based on Bezier interpolation of salient control points [8].

In [8] it has been pointed out that patients are not always aligned according to the standard procedures, and consequently the lung fields may be projected affinely onto the radiographic film. In addition external objects used for their monitoring or support, such as tubes and clips may also be present, affecting the performance of the current lung field detection methodologies. This is a usual situation in intensive care, where portable x-ray devices are used for capturing radiographs from patients immobilized in bed, possibly operated, intubated and connected to monitoring devices [2]. The unsupervised methodology proposed in [8] addresses these issues; however, it sometimes produces implausible lung field shapes since it does not pose any shape constraints.

Among the various lung field segmentation methodologies [1], the shape-constrained deformability of ASMs makes them a competent candidate for handling the segmentation of misaligned lung fields. According to the original ASM approach [11] the shape of an image region is represented by the principal components of landmark point vectors, whereas the grey-level appearance of that region is limited to its border, and consists of the normalized first derivative of the grey-level intensity profiles centred at each landmark that run perpendicular to the region's contour. This formulation makes evident that ASMs are quite sensitive to weak lung field boundaries and to the presence of external objects which affect the derivatives of the intensity profiles.

In this paper we propose a novel approach to ASM-based lung field segmentation that copes with the afore-mentioned issues. The proposed approach utilizes the selective thresholding scheme originally proposed in [8] so as to: a) derive the pose of the initial shape model, and b) shield the ASM from leaking into the lung fields.

The rest of this paper consists of four sections. In section 2 a brief description of the selective thresholding algorithm is provided. The proposed ASM approach is presented in section 3. In section 4 the results of its experimental evaluation are presented, whereas in the last section the conclusions of this study are summarized.

II. Selective Thresholding

Let I be a new chest radiograph of size $N \times M$ pixels, which is uniformly sampled from top to bottom with s_h non-overlapping rectangular windows of $h \times M$, pixels, where $h<N$. For each sample an average horizontal profile of grey-level intensities is estimated. For each profile a local maximum is selected as a spinal cord point according to [8]. The selective thresholding algorithm proceeds as follows:

Step 1. Sample the radiograph across spinal cord:

- For each of the s_h points detected on the spinal cord
  - Acquire a square sample of x^2 pixels.

Manuscript received July 10, 2009. This work was supported in part by the European Commission's Seventh Framework Information Society Technologies (IST) Programme, Unit ICT for Health, project DEBUGIT (no. 217139).

D.K. Iakovidis and M. Savelonas are with Department of Informatics and Computer Technology, Technological Educational Institute of Lamia, 3rd klm PEO Lamias-Athinon, 35100, Lamia, Greece {dimitris.iakovidis, msavelonas}@ieee.org.

978-1-4244-5379-5/09/$26.00 ©2009 IEEE

- For each sample i=1,…,s_h:
  - Calculate its intensity histogram h_i,
  - Select a set of histogram components ph_i centred at its highest peak.

Step 2. Accumulate the values ph_i from all samples into a single histogram H.

Step 3. Find the last non-zero component m of H.

Step 4. Generate an output image $T(I)$ from I as follows:

- Set the intensities of I that correspond to the non-zero components of H, to zero.
- Set the intensities of I that are larger than m, to zero.
- Set all non-zero intensities to one to obtain a binary image $B_T(I)$ (Fig.1b).

The intensities that are larger than m are subtracted from I because they are unlikely to belong to the lung fields since the spinal cord is generally brighter than both normal lung parenchyma and consolidations [12]. Such regions may include dense objects used for patient's monitoring or support.

III. ASM Aided by Selective Thresholding

The shape of a lung field can be described by n landmark points $(x_1,y_1),\ldots,(x_n,y_n)$ forming a shape vector $x=(x_1,y_1,\ldots,x_n,y_n)^T$. The ASM approach [11] applies principal component analysis (PCA) to build a shape model from a set of training shape vectors of ground truth lung field boundaries in different chest radiographs. The shape model is represented by the covariance matrix of the shape vectors $\mathbf{C}_\mathbf{x}$ from which t eigenvectors ϕ_i, i=1,…,t corresponding to the largest eigenvalues λ_i, are estimated. The value of t is determined as the smallest t for which the following inequality holds [4]:

$$\sum_{i=1}^{t}\lambda_i \geq f_v \sum_{i=1}^{2n}\lambda_i \qquad (1)$$

where f_v is the desired percentage of shape variation to be represented by the t principal eigenvectors. The eigenvectors form the matrix $\Phi=(\phi_1|\phi_2|...|\phi_t)$ which is used for the approximation of a shape $\mathbf{x}$ in:

$$\mathbf{x}=\bar{\mathbf{x}}+\Phi\cdot\mathbf{b}_\mathbf{x} \qquad (2)$$

where $\bar{\mathbf{x}}$ denotes the mean of N training shape vectors, and $\mathbf{b}_\mathbf{x}$ holds the shape parameters, estimated by $\mathbf{b}_\mathbf{x}=\Phi^\mathrm{T}(\mathbf{x}-\bar{\mathbf{x}})$.

In addition to the shape, the ASM models also the local appearance of the image region around each landmark. The local appearance model is represented by the mean $\bar{\mathbf{d}}_i$ and the covariance matrix $\mathbf{C}_{\mathbf{d}i}$ of the normalized first derivatives $\mathbf{d}_i=(d_{i1},d_{i2},...,d_{i2k})^\mathrm{T}$, k>0, of image intensity profiles $\mathbf{g}_i=(g_{i1},g_{i2},...,g_{i2k+1})^\mathrm{T}$. The latter are sampled around each landmark i=1,…,n over the N training shapes. The trained ASM is then applied on a new chest radiograph after proper initialization and evolves to detect the lung field boundaries.

A. Initialization

The proposed approach applies a novel ASM initalization scheme to obtain the initial position, the rotation, and the scale of the mean shape of each lung field so that the ASM algorithm begins to evolve from an initial model that is close to the target lung field boundaries.

Initially, a set of points belonging to the left and to the right side of the ribcage are selected according to [8]. The outer left and right points of the ribcage are interpolated by Bézier curves and connected, so as to segment I into two regions. The Bézier curves have been considered for their intuitiveness and their robustness to outliers [8],[10]. The segmented image is binarized so that the pixel values under the curve are equal to one, and the pixel values over the curve are equal to zero. This is denoted as $B_I(I)$ (Fig. 1c).

The two binary images $B_I(I)$ and $B_T(I)$ are then combined using $B_{IT}(I)=B_I(I)\wedge B_T(I)$ to produce a new binary image $B_{IT}(I)$ (Fig. 1d), which can be considered as a rough mask for the two lung fields. This mask is further divided by the spinal cord points into two parts; a left part $B_{IT}^L(I)$ and a right part $B_{IT}^R(I)$, corresponding to each of the two lung fields, such that $B_{IT}(I)=B_{IT}^L(I)\vee B_{IT}^R(I)$.

The centre of mass of each part is chosen for the positioning of the centre of mass of the mean shape of each lung field. The centre of mass is estimated by the two first order geometric moments of the binary image [13]. The rotation of both mean shapes is determined by the angle θ between the line obtained with linear regression [14] from the spinal cord points and the vertical axis of the image. Given a fixed position and rotation angle of the mean shape of the left and the right lung field, the corresponding lung field model is iteratively scaled up until it reaches a maximum overlap with the shapes of the non-zero regions of $B_{IT}^L(I)$ and $B_{IT}^R(I)$, respectively. The overlap ω between the areas of two shapes; a_1 and a_2 is defined by [15]:

$$\omega=\frac{a_1\cap a_2}{a_1\cup a_2} \qquad (3)$$

The translation, rotation and scaling of the shape model is realized by the well-known geometric transformation applied on each landmark (x, y), whereas initially $\mathbf{b}_\mathbf{x}^i=\mathbf{0}$, i=L,R.

B. Evolution

The initialized ASM evolves according to a simple iterative scheme [11]. Each landmark can move along a direction perpendicular to the contour by s positions on either side of the contour, evaluating 2s+1 positions, in total. The new position (x_i',y_i') of each landmark i=1,…,n, on the search direction, is determined as the one minimizing the

Mahalanobis distance between the vector of the normalized first derivatives estimated from the $2s+1$ pixel intensity profile centred at each of the possible new landmark positions (x'_{ij}, y'_{ij}), $i=1,\ldots,n$, $j=1,\ldots,2s+1$, and $\bar{\mathbf{d}}_i$. After all the landmarks are updated, the shape model is fitted to the new landmarks.

The proposed approach to ASM evolution takes into account that the lung fields lie in a contiguous region of non-zero pixels in $B_T(I)$ and prohibits the model to evolve towards these regions in I. This way leaking inside the lung fields can be avoided. The initialization of the model as described in the previous subsection, and the incorporation of multiresolution local appearance models helps the algorithm to avoid trapping into irrelevant regions. Moreover, the a priori shape information included in the ASM helps the algorithm to achieve a plausible delineation of the lung fields even if part of them remains joint with their surroundings, or artifacts are present, in $B_T(I)$.

The proposed ASM evolution algorithm proceeds as follows:

Step 1. Update landmark positions:

- For each possible new landmark position (x'_{ij}, y'_{ij}), $i=1,\ldots,n, j=1,\ldots,2s+1$:
  - Calculate a profile of normalized first derivatives $\mathbf{d}'_{ij} = (d_{ij1}, d_{ij2}, \ldots, d_{ij2k})^{\mathrm{T}}$ on I, centred at this landmark position perpendicular to the contour.
  - From all $\mathbf{d}'_{ij}$, such that $T(I(x'_{ij}, y'_{ij})) = 0$, find $\mu_{\min}(\mathbf{d}'_i) = \min_{j=1,\ldots,2s+1}(\mu(\mathbf{d}'_{ij}))$.
  - $(x'_i, y'_i) = (x'_{ij}, y'_{ij})$ is the new position of landmark i.

Step 2. Fit the current shape model to the updated landmarks:

- Set $\mathbf{x}' = (x'_1, y'_1, \ldots, x'_n, y'_n)^{\mathrm{T}}$.
- Calculate the new model parameters for $\mathbf{x}'$ by solving Eq. (2) for $\mathbf{b}_{\mathbf{x}'}$.
- Constrain each component $|b_l| < c\sqrt{\lambda_l}$ of $\mathbf{b}_{\mathbf{x}'}$, $c>0$, $l=1,\ldots t$, to ensure plausible shapes.

Step 3. Repeat steps 1 to 3 until a proportion of p_{close} of points ends up within $s/2$ of its previous position, or M_{max} iterations are reached.

Step 4. Move to the next resolution level.

Step 5. Repeat steps 1 to 5 until the finest resolution level R_{max} is reached.

IV. Results

The experimental evaluation of the proposed approach was performed on a set of 58 anonymous chest radiographs obtained with a portable x-ray device from critically ill patients with pulmonary bacterial infections manifested as consolidations. The radiographs were digitized at 8 bits per pixel and have been downscaled to fit a 256×256-pixel bounding box. The parameters considered include $w=h=9$, $x=32$, $f_v=0.98$, $R_{max}=3$, $M_{max}=30$, $s=2$ and $c=2$.

The performance of the proposed methodology was assessed in terms of Ω, a widely accepted measure of accuracy for binary segmentation tasks [9]:

$$\Omega = \frac{TP}{TP + FP + FN} \tag{4}$$

where TP stands for true positive (the area classified as lung by both the proposed methodology and the expert), FP for false positive (area classified as background by the expert and as lung by the proposed methodology) and FN for false negative (area classified as lung by the expert and as background by the proposed methodology). This measure is more suitable measure of segmentation performance than the accuracy used in [8], since the latter counts TN pixels as correctly detected, providing deceptively high results in cases of relatively small target objects.

The results from the application of the proposed and the original ASM approach on the available dataset are illustrated in Fig. 2. The average values of Ω presented in this figure are estimated by the leave-one-out cross-validation scheme. The last column presents the average value of Ω obtained with the unsupervised Bézier interpolation method proposed in [8]. Indicative segmentations obtained with the three methodologies tested are illustrated in Fig. 3. This figure shows clearly that the proposed methodology avoids contour leaking, whereas it achieves more plausible delineation than the Bézier interpolation method without missing the costophrenic angles. Moreover, it should be noted that in our experiments the region of the lung fields overlapped by the heart is not excluded because it may also contain abnormal findings [3].

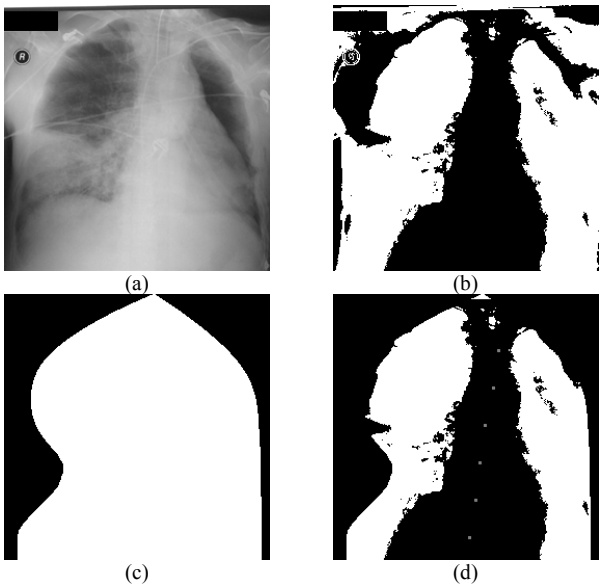

Fig. 1. Images obtained from the intermediate steps of the proposed approach. (a) Radiograph I, (b) $B_T(I)$, (c) $B_I(I)$, (d) $B_{IT}(I) = B^L_{IT}(I) \vee B^R_{IT}(I)$, where $B^L_{IT}(I)$ and $B^R_{IT}(I)$ contain the left and the right part of $B_{IT}(I)$ respectively, as these parts are divided by the grey points corresponding to the spinal cord.

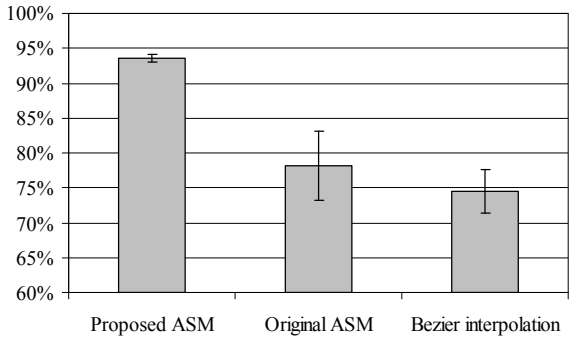

Fig. 2. Comparative results obtained with the three lung field segmentation methodologies tested.

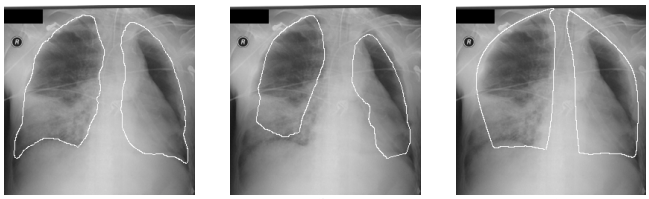

(a) (b) (c)

Fig. 3. Representative segmentations of the lung fields from the radiograph illustrated in Fig. 1, obtained with (a) the proposed ASM approach, (b) the original ASM approach, and with (c) the Bezier interpolation methodology proposed in [8].

V. CONCLUSIONS

We proposed a novel approach to the segmentation of the lung fields in chest radiographs based on ASMs. The proposed approach is aided by a grey-level selective thresholding scheme which prohibits the shape's contour to leak into the lung fields even if the lung field boundaries are weakly defined. This advantage over the original ASM approach was validated by the results of our experimentation. In addition, the results indicate that the proposed approach is capable of segmenting affinely projected lung fields due to patient's misalignment with the portable x-ray device, and it is resistance to the presence of external objects used for patient's monitoring or support.

Future work includes further experimentation with a larger set of chest radiographs, which is currently being annotated by the experts, and fine tuning. The developed methodology will be integrated into a multimodal data mining system for adverse events detection, which will be capable of co-evaluating radiographic findings of patients with bacterial infections [16].

ACKNOWLEDGMENT

Great thanks to G. Papamichalis, M.D. who generously offered his help and advice on the medical aspects of this study. The radiographs have been provided in anonymized form by the General Hospital of Athens "Sotiria" for the purposes of the project DEBUGIT.

REFERENCES

[1] B.V. Ginneken, B.T.H. Romeny, and M.A. Viergever, "Computer-Aided Diagnosis in Chest Radiography: A Survey," *IEEE Trans. Med. Imag.*, vol. 20, no. 12, 2001, pp. 1228-1241.

[2] F.S. Bongard, and D.Y. Sue, *Current Critical Care Diagnosis & Treatment*, 2nd ed., McGraw-Hill/Appleton & Lange, 2002.

[3] N.L. Müller, T. Franquet, K.S. Lee, C. Isabela, and S. Silva, *Imaging of Pulmonary Infections*, Lip. Williams & Wilkins, 2006.

[4] B.V. Ginneken, S. Katsuragawa, B.T.H. Romeny, K. Doi, and M.A. Viergever, "Automatic Detection of Abnormalities in Chest Radiographs Using Local Texture Analysis," *IEEE Trans. Med. Imag.*, vol. 21, no. 2, 2002, pp. 139-149.

[5] X. Xie, X. Li, S. Wan, and Y. Gong, "Mining X-Ray Images of SARS Patients," in G.J. Williams and S.J. Simoff (Eds.) *Data Mining*, LNAI, vol. 3755, 2006, pp. 282-294.

[6] S. Chen, L. Cao, J. Liu and X. Tang, "Automatic Segmentation of Lung Fields from Radiographic Images of SARS Patients Using a New Graph Cuts Algorithm," *Proc. Int. Conf. Pattern Recognition (ICPR)*, vol. 1, 2006, pp. 271-274.

[7] P.H. Meyers, H.C. Nice, C.M. Becker, N.J. Nettleton, J.W. Sweeney, and G.R. Meckstroht, "Automated Computer Analysis of Radiolographic Images," *Radiology*, vol. 13, 1964, pp. 1029-1034.

[8] D.K. Iakovidis, and G. Papamichalis, "Automatic Segmentation of the Lung Fields in Portable Chest Radiographs Based on Bézier Interpolation of Salient Control Points," *Proc. IEEE Int. Conf. on Imag. Sys. Tech.*, Greece, 2008, pp. 82-87.

[9] B.V. Ginneken, M.B. Stegmann, M. Loog, "Segmentation of Anatomical Structures in Chest Radiographs using Supervised Methods: A Comparative Study on a Public Database," *Medical Image Analysis*, vol. 10, 2006, pp. 19-40.

[10] R.H. Bartels, J.C. Beatty, and B.A. Barsky, Bézier Curves. Ch. 10 in *An Introduction to Splines for Use in Computer Graphics and Geometric Modelling*, San Francisco, CA: Morgan Kaufmann, 1998, pp. 211-245.

[11] T. Cootes, C. Taylor, D. Cooper, and J. Graham, "Active Shape Models - Their Training and Application," *Comp. Vis. and Image Understanding*, vol 61, no. 1, 1995, pp. 38-59.

[12] R.A. Novelline, *Squires's Fundamentals of Radiology*. Cambridge: Harvard University Press, 1997.

[13] R.J. Prokop, A.P. Reeves, "A Survey of Moment-based Techniques for Unoccluded Object Representation and Recognition," *Graph. Mod. Imag. Proc.*, vol. 54, no. 5, 1992, pp. 438–460.

[14] D.C. Montgomery, E.A. Peck, G. Vining, I*ntroduction to Linear Regression Analysis*, 3rd ed., Wiley-Interscience, 2003.

[15] W.R. Crum, O. Camara, L.G. Hill, "Generalized Overlap Measures for Evaluation and Validation in Medical Image Analysis", *IEEE Trans. Med. Imag.*, vol. 25, no. 11, 2006, pp. 1451-1461.

[16] C. Lovis, D. Colaert, V.N. Stroetmann, "DebugIT for Patient Safety-Improving the Treatment with Antibiotics through Multimedia Data Mining of Heterogeneous Clinical Data," *Stud. Health Technol. Inform.*, vol. 136, 2008, pp. 641-646.